ADVANCED FUNCTIONAL MATERIALS
www.afm-journal.de

Near-Infrared Light-Absorptive Stealth Liposomes for Localized Photothermal Ablation of Tumors Combined with Chemotherapy

*Menghuan Li, Cathleen Teh, Chung Yen Ang, Si Yu Tan, Zhong Luo, Qiuyu Qu, Yuanyuan Zhang, Vladimir Korzh, and Yanli Zhao**

Although near-infrared (NIR) light-absorbing organic dyes have recently been proposed for photothermal ablation of tumors, their clinical applications have often been hampered by problems such as low water solubility and minimal tissue absorption. Rapid development of nanotechnology provides various novel nanostructures to address these issues. In this work, doxorubicin (DOX)-loaded stealth liposomes are engineered through the incorporation of an NIR-absorptive heptamethine indocyanine dye IR825 into the thermoresponsive liposomes for photothermal/chemo combined cancer therapy. It is demonstrated that the lipid nanostructure can enhance the bioavailability of water-insoluble IR825 for efficient photothermal treatment, while delivering the anticancer drug doxorubicin to achieve simultaneous anticancer medication. The combined treatment of photothermal ablation and chemotherapy synergistically improves the overall cancer cell killing efficiency, which can be of future clinical interest.

1. Introduction

The emergence of nanotechnology has profoundly affected the anticancer research. Innovative nanomaterials could be employed to greatly enhance the efficacy of conventional chemotherapy by enabling many alternative treatment strategies that were traditionally considered unreliable. Photothermal therapy is one of those techniques that have been reactivated recently thanks to the development of nanotherapeutics.[1] By using photoinduced localized hyperthermia to destroy the cancer cells, therapeutic efficacy of photothermal ablation is theoretically unaffected by the drug resistance of cancer cells evolved through somatic evolution, which is unlike chemotherapy.[2,3] The translation of photothermal ablation therapy from research to clinical trials has long been hampered by nondiscriminative light absorption from both the healthy tissue and tumor. This issue could be solved by the introduction of nanosized photothermal agents and new optical devices. These innovations could provide precise localization and intensity control on photothermal heating,[4–6] which substantially improve the outcome of photothermal ablation therapy. Amongst all the photothermal agents that have been developed, near-infrared (NIR)-absorbing nanomaterials have drawn extensive interest.[7–9] These nanomaterials could interact with deep tissue-penetrating NIR light, allowing for localized heat deposition in the target site and minimized collateral damage to adjacent healthy tissues. However, most of the photothermal agents used in the NIR range are inorganic nanomaterials that cannot be easily degraded or excreted in biological environment.[10] Thus, it is of great importance to develop NIR-absorbing organic nanosystems to reduce the long-term risks of photothermal treatment.

IR825 is a cationic heptamethine indocyanine dye with high absorption coefficient in the NIR range as well as negligible quantum yield, meaning that most of the photon energy it absorbs would be released through nonradiative relaxation process.[11] The potent light-to-heat conversion efficiency of IR825 makes it a potential candidate for photothermal therapy. However, its utilization in anticancer applications has been limited by several inherent issues, such as poor water solubility, inefficient intrabody recirculation and negligible tissue uptake. To overcome these drawbacks, new strategies for IR825 modification and delivery have been proposed and put into practice. For example, IR825 was encapsulated within PEGylated micelles to significantly enhance its water solubility and bioavailability.[11,12] These studies provide useful insights into the

M. Li, C. Y. Ang, S. Y. Tan, Dr. Z. Luo, Q. Qu, Y. Zhang, Prof. Y. Zhao
Division of Chemistry and Biological Chemistry
School of Physical and Mathematical Sciences
Nanyang Technological University
21 Nanyang Link
Singapore 637371, Singapore
E-mail: zhaoyanli@ntu.edu.sg
M. Li, Prof. Y. Zhao
School of Materials Science and Engineering
Nanyang Technological University
Singapore 639798, Singapore
Dr. C. Teh, Dr. V. Korzh
Laboratory of Fish Development Biology
Institute of Molecular and Cell Biology
61 Biopolis Drive
Singapore 138673, Singapore

DOI: 10.1002/adfm.201502469

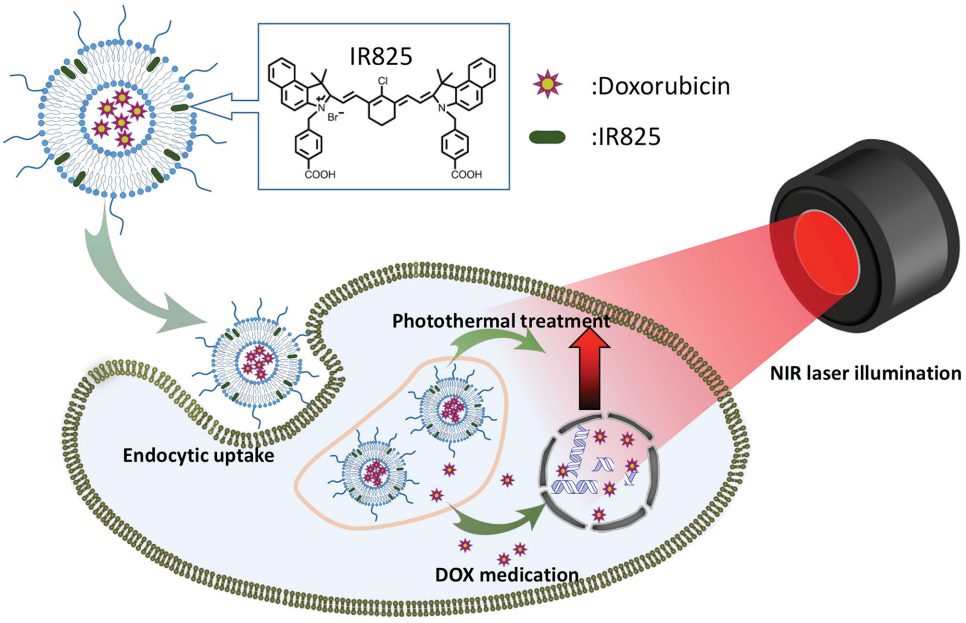

Figure 1. Schematic illustration showing the structure and action mechanism of NIR-absorptive DOX-loaded stealth liposome.

design and fabrication of photothermal therapeutic nanosystems with IR825.

Due to the extremely hydrophobic nature of IR825, it is very difficult to be used in common nanoparticle-based drug delivery systems without substantial modifications at a molecular level.[13] As it could be readily dissolved in short-chain alcohols and fatty acids, it is possible to incorporate IR825 into nanosized delivery vehicles consisting of at least a hydrophobic oleic phase. Amongst the current nanocarriers that meet these criteria, liposomes stand out for their versatility and biosafety. Liposomes are usually spherical nanovesicles comprised of highly biocompatible lipid bilayer shells enclosing aqueous interior compartments, which can be easily degraded in physiological conditions and cleared rapidly from the body.[14] Liposomes have been used as effective and versatile delivery nanosystems for a variety of bioactive substance in clinical practice, due to their lipid/aqueous biphasic nature.[15] Both hydrophilic and lipophilic compounds could be accommodated in liposomes depending on their solubility in liposome components.[16] For instance, asymmetric hydrophobic molecules such as paclitaxel and camptothecin could be reliably entrapped within the lipid bilayer of liposomes,[16,17] while hydrophilic molecules such as doxorubicin (DOX) could be contained in the aqueous interior.[18] Thus, it is theoretically possible that liposomes could accommodate IR825 and DOX molecules simultaneously for photothermal and chemo combinational cancer therapy.

Ever since the first discovery of liposomes in 1961,[19] many liposomal formulations have emerged, offering advanced and versatile features aside from the basic drug encapsulation capability. Specifically, PEGylated lipid has been developed as a countermeasure against the fast clearance of liposomes in vivo,[20,21] which could significantly prolong the circulation time of liposomes in physiological environment while having negligible impact on their release behavior.[22] In addition, the polyethylene glycol (PEG) corona could reduce the susceptibility of liposomes to self-aggregation and antibody opsonization.[23] Another noteworthy example is thermoresponsive liposomal formulation.[24,25] These liposomes are comprised of primarily two chemical components, namely, 1,2-dipalmityol-*sn*-glycero-3-phosphocholine (DPPC) and 1,2-distearoyl-*sn*-glycero-3-phosphocholine (DSPC), and have a phase transition temperature range of 39–42 °C,[26] above which the gel-like lipid bilayer becomes more disordered, causing disruptions in the domain boundaries so that the aqueous content may escape through the lipid membrane. This unique temperature sensitivity could reduce the drug leakage during the transportation of liposomes in physiological environment, which is preferable for successful chemotherapy.[27] Overall, these technical advances could improve the delivery efficiency of liposomal nanocarriers as well as their pharmacokinetics.

In this work, an NIR-absorptive stealth liposome (NSL) was successfully developed by entrapping IR825 within the liposomal phospholipid bilayer of PEG-protected DPPC/DSPC thermoresponsive liposome, and its physical/chemical properties were thoroughly investigated. In addition to photothermal agent IR825, a widely used anticancer drug DOX was loaded into the aqueous interior of NSL. We hypothesized that this liposome structure could stably complex a large amount of IR825 and facilitate cellular uptake of its content primarily through robust endocytosis as well as liposome fusion with the cell membrane,[28] which would ensure subsequent efficiency of NIR photothermal therapy. Simultaneous chemotherapy could be achieved by the release of the second encapsulated cargo DOX upon intracellular degradation of the NSL (**Figure 1**). This combinational therapeutic effect of DOX-loaded NSL was evaluated in HeLa cells and further validated in zebrafish liver hyperplasia models.[29]

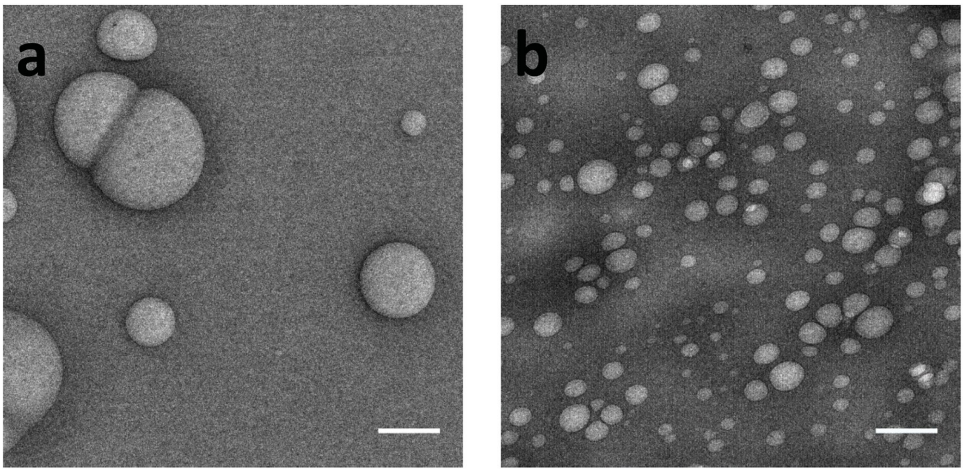

Figure 2. TEM images of IR825-containing stealth liposomes. a) Liposomes freshly prepared through ultrasonication. b) Liposomes after thermally extruded 21 times at 60 °C. The calculated mean diameter was 91.3 ± 7.5 nm. Scale bars are 200 nm.

2. Results and Discussion

As shown from dynamic light scattering (DLS) results (Figure S1, Supporting Information), the NSL prepared via the film-hydration and sonication/extrusion strategy showed excellent morphological homogeneity with an average diameter below 100 nm, which is consistent with transmission electron microscopy (TEM) characterizations (**Figure 2**). These liposomes have a slightly negative surface charge of −3.68 mV (Figure S1, Supporting Information), which is common for liposomal formulations containing 1,2-distearoyl-*sn*-glycero-3-phosphoethanolamine-*N*-PEG (DSPE-PEG) due to those negatively charged phosphate groups.[30]

The incorporation of IR825 in the lipid bilayer was confirmed by UV–vis spectrum. As the IR825 dye is water insoluble, it was dissolved in methanol when monitoring its optical absorption. It could be observed from **Figure 3** that the main absorption peak of IR825 was located at around 825 nm. For blank liposomes without IR825, no significant optical absorption was observed in the scanning range. However, when IR825 was added into the formulation, one intense peak appeared in the vicinity of 840 nm with several other peaks at around 400 and 600 nm. The observation of these characteristic IR825 peaks in UV–vis spectrum demonstrated that IR825-containing stealth liposomes were successfully prepared. It is important to note that the main absorption peak of the IR825 species incorporated in the liposomes slightly redshifted in comparison with that of the free dye in methanol. This redshift could be explained by increased dielectric constant from methanol (32.7) to water (80.1).[11] Moreover, the DOX encapsulation in the liposomes was confirmed and quantified by the fluorescence detection after the liposome disruption. With a DOX concentration of 5 mg mL^{-1} in the hydration solution, the DOX encapsulation capacity in the NSL was found to be around 1.5 wt%.

Following the optical characterizations, the temperature rising of the liposome solution under NIR laser illumination was monitored to investigate its photothermal capability. It was found that after only 1 min of direct laser illumination, the temperature of the NSL solution increased drastically by almost 20 °C. After 4 min of continuous illumination, the temperature of the sample solution rose up to 58 °C and remained at this level, while that of the dextrose solution as a control group was still around room temperature under the same illumination conditions. By comparing the temperature increments of the sample and control solutions, it revealed that the NSL retained high light-to-heat conversion efficacy of IR825 as well as high photothermal capability in the first biological window.

To evaluate the thermostability of the NSL, the critical phase transition temperature of its lipid bilayer was investigated using differential scanning calorimeter (DSC). The heat flow plot revealed that the melting of the lipid bilayer in the NSL initiated at 45 °C (Figure S3, Supporting Information), which was slightly higher than the phase transition temperature reported for conventional thermoresponsive DPPC/DSPC liposomes (39–42 °C).[25,26,31–33] The elevated melting temperature (T_m) indicated that the introduction of IR825 dye into the liposomes augmented the stability of the lipid membrane against the

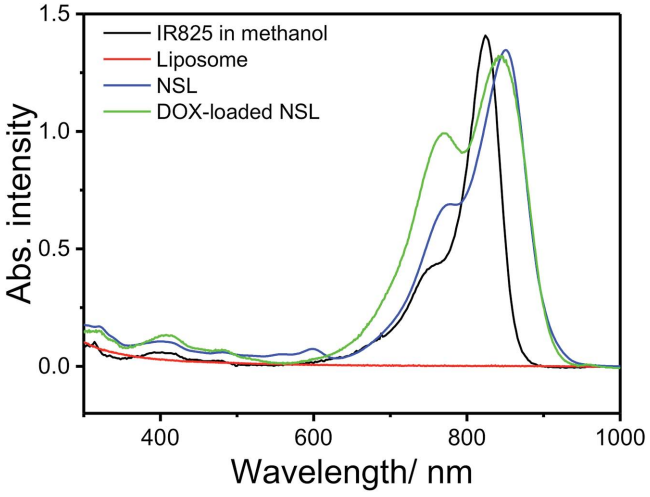

Figure 3. UV–vis absorption spectra of IR825 in methanol (0.01 mg mL^{-1}), bare stealth liposome (1 mg mL^{-1}), NSL (1 mg mL^{-1}), and DOX-loaded NSL (1 mg mL^{-1}) solutions.

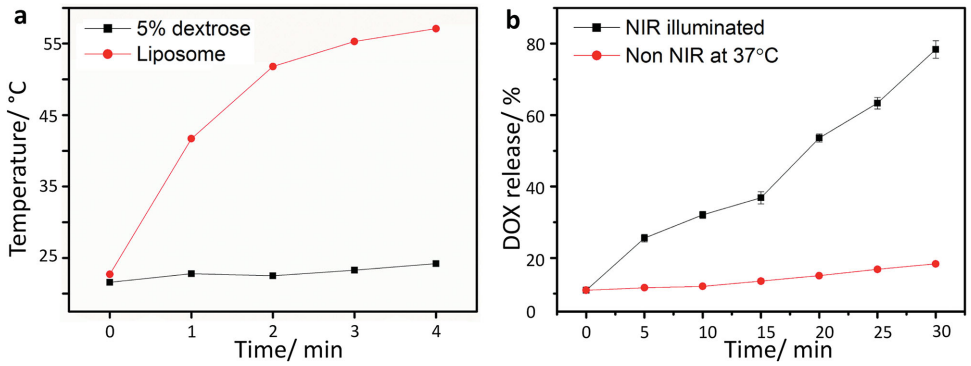

Figure 4. a) Heating curves of the hydration solution (5% dextrose) and the NSL solution upon continuous NIR laser illumination at a laser power density of 0.5 W cm^{-2}. b) DOX release profiles of DOX-loaded NSL at physiological temperature and under NIR light irradiation (power density: 0.5 W cm^{-2}), respectively.

structural disruption caused by temperature escalations. More importantly, with a T_m above physiological temperature of 37 °C, it is highly promising that the liposomes could reduce the leakage of encapsulated anticancer drugs under unstimulated conditions.

Based on the DSC results, time-dependent release profile of the DOX-loaded NSL was measured to investigate its structural stability at physiological temperature conditions. The release profile was monitored using conventional dialysis method.[34] The DOX-loaded NSL solution was contained inside dialysis membranes with a molecular weight cutoff of 3000, which could effectively isolate the released DOX from the NSL. It was observed that the DOX-loaded NSL was capable of retaining its DOX cargo in isotonic buffer solution (5% aqueous dextrose solution) at physiological temperature and that less than 10% of total encapsulated DOX was leaked after 30 min of incubation at 37 °C, similar to previously reported thermoresponsive liposomal formulations.[27,35–37] However, when the NIR laser illumination was applied, a drastic increase of DOX fluorescence was detected in the release medium. With an NIR illumination density of 0.5 W cm^{-2}, the DOX-loaded NSL released more than 20% of total encapsulated DOX in the first 10 min, and eventually the release percentage reached more than 80% in 30 min (**Figure 4**). These results demonstrated the good stability of the liposomes at normal body temperature as well as the capability of enhanced cargo release when the liposomes were stimulated with photothermal heating.

Photothermal heating curves and the DOX release profiles of the NSL in isotonic buffer solution indicated its potential use in both photothermal therapy and chemotherapy. To confirm the hypothesis, in vitro experiments with the NSL were carried out on HeLa cancer cell line. Liposomes have excellent cellular bioavailability due to chemical and structural similarities between the lipid bilayer and the cell membrane. This bioavailability facilitates cellular uptake of liposomes by multiple pathways such as direct liposome-cell fusion, lipid exchange, phagocytosis, and endocytosis.[28] The uptake of NSL in live HeLa cells was assessed using confocal laser fluorescence spectroscopy. The anticancer drug, DOX, with its intrinsic red fluorescence was used as an indicator for successful cellular internalization. HeLa cells were incubated with free DOX and DOX-loaded NSL in the culture medium respectively for comparison. As shown in **Figure 5**a, after 4 h of incubation with free DOX (3 μg mL^{-1}), red fluorescence was enriched in the cell nuclei and their vicinity, which was consistent with the findings from previous studies.[38,39] For HeLa cells that were exposed to DOX-loaded NSL with equivalent DOX concentration, DOX fluorescence was detected throughout the cell cytoplasm and nuclei. As compared with free DOX, the DOX intensity in the cell nuclei was weaker when exposed to DOX-loaded NSL. The distinctive DOX fluorescence pattern of DOX-loaded NSL in HeLa cells suggested that some DOX molecules might still remain encapsulated within the liposomes after 4 h of incubation. The observations also indicated that DOX-loaded NSL was successfully internalized in HeLa cells through predominant endocytic pathway as well as direct membrane fusion.

In order to correlate the internalization of DOX-loaded NSL with its proapoptotic effect on HeLa cells, the cells treated with DOX-loaded NSL were stained with Annexin V-fluorescein isothiocyanate (FITC) probe to assess the extent of apoptosis using flow cytometry (Figure 5b,c and Figure S4 in the Supporting Information). According to Figure 5b, the flow cytometric analysis of the cells that underwent 4 h of incubation with DOX-loaded NSL solution at 37 °C revealed a drastic increase in median DOX fluorescence intensity, which was almost 13-fold stronger than that of the blank control, suggesting that the internalization of DOX-loaded NSL into HeLa cells occurred. Correspondingly, chemotherapeutic capability of released DOX was revealed in Figure 5c, where median FITC fluorescence intensity of the whole cell population in DOX-loaded NSL group increased significantly by around 14-fold after incubation of 4 h. The confocal laser fluorescence spectroscopy and flow cytometry results collectively demonstrated that DOX-loaded NSL could be readily internalized by the HeLa cell line and induce the cell apoptosis attributed to the release of liposomal DOX. 3-(4,5-Dimethylthiazol-2-yl)-2,5-diphenyltetrazolium bromide (MTT) assay was subsequently carried out to quantitatively assess the tumoricidal effect of the NSL. Its photothermal ablation capability was studied first. As depicted in **Figure 6**a, no obvious cytotoxicity (cell viability >90%) was detected in HeLa cells even treated with an NSL concentration of 120 μg mL^{-1} in the absence of NIR illumination, which was a good indicator for the biosafety of the NSL. Contrastingly, a sharp increase in the cell death rate with only 14% of the cell survival was observed

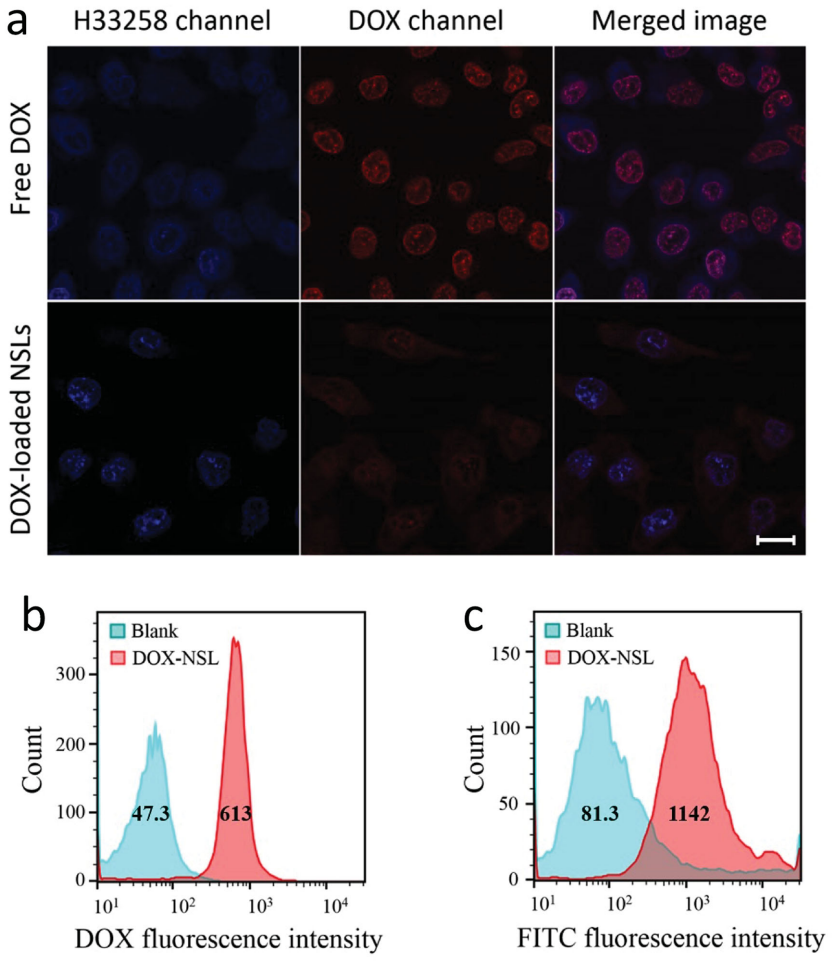

Figure 5. a) Confocal laser fluorescence spectroscopy images of live HeLa cells incubated with free DOX (3 μg mL^{-1}) or DOX-loaded NSL (200 μg mL^{-1}) solutions. The cell nuclei were stained with H33258. Scale bar is 10 μm. Flow cytometric analysis on the changes of b) DOX and c) FITC fluorescence intensities from HeLa cell line after incubation with DOX-loaded NSL solution (200 μg mL^{-1}). Median DOX and FITC fluorescence intensities of each sample group were also shown.

when the NSL-treated cells were illuminated with NIR laser for 5 min. When the duration of laser illumination was prolonged to 10 min, the cell viability at the NSL concentration of 120 μg mL^{-1} further dropped to 9%. It should also be noted that, at zero concentration of NSL used, the NIR laser illumination did not confer obvious influence to the cells.[40] The comparative analysis of the MTT results supported the in vitro efficacy of NIR triggered photothermal cancer cell ablation with internalized NSL.

By using the same experimental setup, combinational therapeutic efficacy of the DOX-loaded NSL was further inspected on HeLa cell line. Despite of the absence of NIR illumination, a concentration-dependent toxicity was detected on HeLa cells treated with DOX-loaded NSL, where the cell viability eventually fell below 60% upon incubation with 120 μg mL^{-1} of DOX-loaded NSL (Figure 6b), which was comparable to the cytotoxicity of free DOX at an equivalent concentration. In addition, when the NIR laser illumination was applied, a further drop in the cell viability was detected. The cell survival rate was down to 9% after 10 min of laser illumination at the DOX-loaded NSL concentration of 120 μg mL^{-1}. Even though the anticancer property of the liposomal DOX was less obvious as compared with the concurrent NIR-induced photothermal ablation, the cell viability of the cells treated with DOX-loaded NSL was on average lower than that of nonloaded NSL group under similar concentration and illumination conditions. The in vitro results demonstrated that enhanced tumoricidal outcome could be achieved with combined photothermal and chemotherapeutic properties of DOX-loaded NSL.

An additional proof of combinational therapeutic efficacy on solid tumors in vivo was obtained using transgenic zebrafish based mifepristone inducible liver tumor models expressing enhanced green fluorescence protein (EGFP)-kras^{v12} oncogene.[29,41] In comparison with mouse based tumor models commonly used in anticancer research, the zebrafish

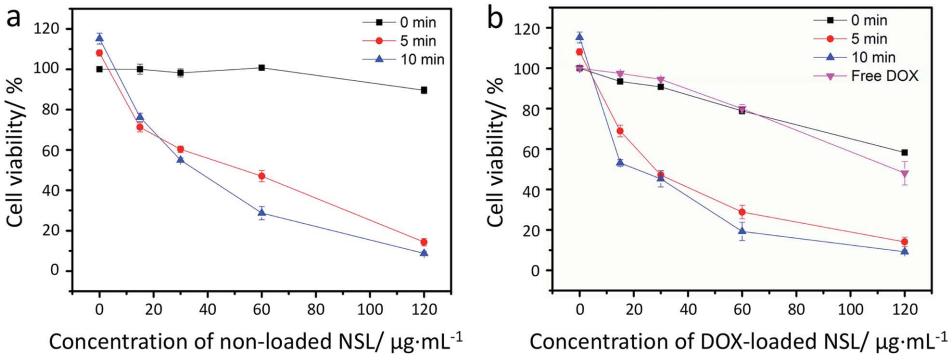

Figure 6. Relative viabilities of HeLa cells incubated with a) nonloaded NSL and b) DOX-loaded NSL at various concentrations without and with NIR laser illumination for 5 and 10 min, respectively. Equivalent concentrations of free DOX solution were used as a control group in Figure 6b. All OD readings at 570 nm were normalized to the mean OD of non-NIR-illuminated control group at zero concentration of nonloaded NSL or DOX-loaded NSL.

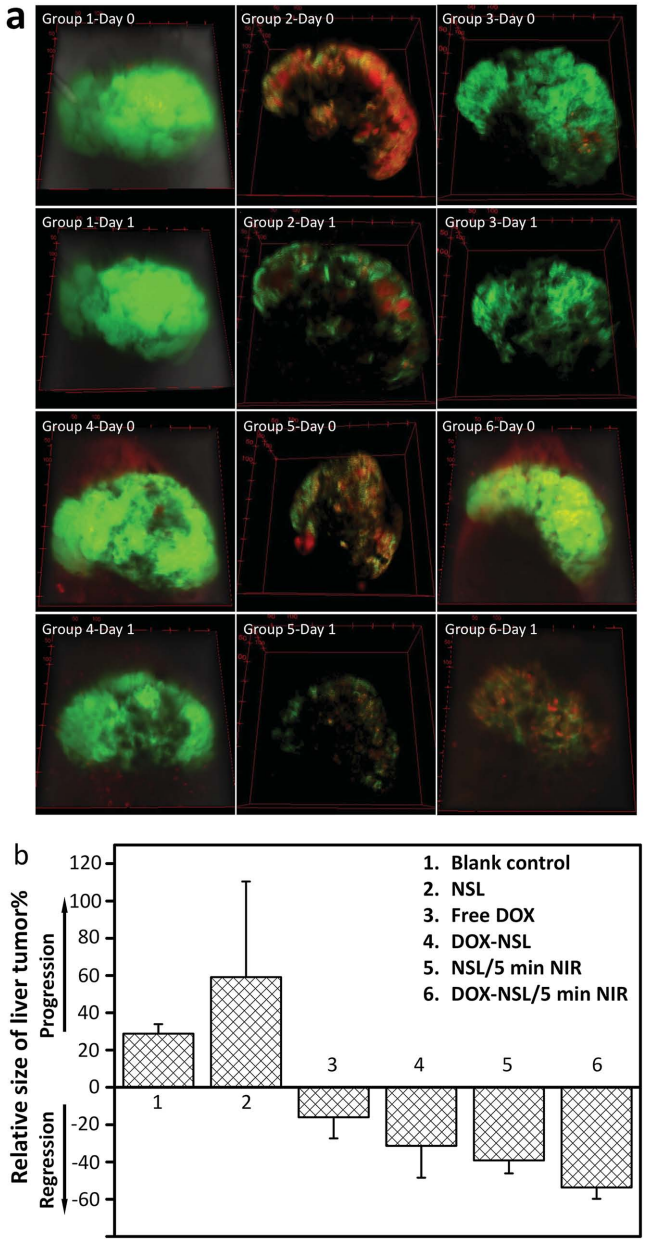

Figure 7. a) 3D fluorescent images of six liver tumor groups before and after treatment for 1 d. The same liver tumor was followed at day 0 and day 1 posttreatment. Images represent typical tumor size detected in each sample group. Group 1: blank control without any treatment, Group 2: treated with nonloaded NSL, Group 3: treated with free DOX, Group 4: treated with DOX-loaded NSL, Group 5: treated with nonloaded NSL under 5 min of NIR illumination, and Group 6: treated with DOX-loaded NSL under 5 min of NIR illumination. Only groups 5 and 6 were treated with NIR laser illumination (power density: 1 W cm^{-2}) for 5 min. b) Changes in the relative tumor volume in each sample group, measured after 1 d posttreatment.

embryo models provide a simplified and intuitive approach to study structural changes of the tumors in response to various anticancer treatments. Specifically, external development and optical translucence of zebrafish larvae could facilitate the real-time monitoring of the tumor damage and correlating the extent of associated tumor progression to the anticancer treatments. In this study, liver tumor-bearing larvae were first divided into six subgroups. Group 1 was untreated liver tumor-bearing larvae as the blank control, Groups 2–4 were injected with nonloaded NSL, free DOX, and DOX-loaded NSL solutions under an equivalent concentration respectively, Group 5 was injected with nonloaded NSL solution and illuminated with 5 min of NIR laser, and Group 6 was injected with DOX-loaded NSL solution and treated with NIR laser illumination for 5 min. Each tumor volume was then assessed by confocal imaging, where images detailing tumor depth in the z direction were compiled and the thickness of each optical slice was fixed at 5.5 μm. 3D fluorescent images of liver tumors in all treatment groups are presented in **Figure 7**a. Liver tumor volumes of all larvae in each group were followed at day 0 and day 1 to detect the variations. Tumor progression associated with increased liver tumor volume was observed in Groups 1 and 2. Decreased tumor volume was detected in Groups 3 and 4, which supported modest tumor regression from the DOX medication. The most severe tumor damage on embryos was observed from Groups 5 and 6, where most of the tumor tissues disappeared after one day under NIR mediated ablation. Moreover, the tumor tissues in these two sample groups presented a dissociated morphology after NIR photothermal treatment. The observations in these two groups demonstrated that the tumor cells suffered severe cellular damage (necrosis and pyknosis) as compared to the unilluminated sample groups. Specifically, the hyperthermia incurred by the NIR photothermal treatment could disrupt the cell membrane and degrade the proteins, causing irreversible damage to the cytoskeletal filaments, all of which would contribute to the prompt cell death.[2] The tumor ablation and growth suppression from the combinational therapy were further demonstrated in greater detail from the video files (Videos 1–6, Supporting Information), where the tomographic fluorescence imaging of the liver tumors before and after various treatments (six groups) was carried out and the results were compared.

Based on 3D fluorescent tumor mapping on live zebrafish embryos (Figure S5, Supporting Information), the relative tumor size change in each sample group was further quantified to reveal the therapeutic efficacy of the NSL in vivo and the obtained results are shown in Figure 7b. The quantitation of liver tumor volume was achieved by summing the volume of each optical slice that made up the liver tumor through the volume estimation plugin in Image J (Volumest). It was found that there was no significant difference of the tumor volume changes between Groups 1 and 2 (significance level: 5%), which evidently indicated that the NSL itself had no apparent toxicity to the living cells. It should also be noted that the average tumor size in Group 4 decreased significantly, which was even more effective than that of free DOX solution (Group 3) at an equivalent concentration. Due to high hydrophilicity and small molecular size, free DOX could easily diffuse out from the injection site and result in the abatement of bioactive drug concentration in tumor, while the liposomal DOX released from DOX-loaded NSL could be retained in the tumor for an extended period of time with high local drug concentration on account of ineffective lymphatic drainage. It was found from Group 6 that the tumor regression was the greatest

among all the sample groups, with negligible collateral damage observed on the living larvae, revealing the enhanced combinational therapeutic effect of DOX-loaded NSL under NIR illumination. All these results collectively demonstrated that the combination of DOX-loaded NSL and NIR laser illumination significantly improved the eventual therapeutic outcome on zebrafish liver hyperplasia models, providing useful insights for combinational treatment of solid tumors on more advanced animal cancer models.

3. Conclusions

In summary, NIR-absorptive stealth liposomes have been successfully prepared as combinational therapeutic agents for the cancer treatment. Hydrophobic organic dye IR825 has been incorporated into these liposomes, through which its bioavailability has been significantly improved. The IR825-containing liposomes (NSL) could serve as the nanocarriers for intracellular delivery of anticancer drug DOX, and at the same time as an effective photothermal agent upon NIR laser illumination. It has been confirmed both in vitro and in vivo that the DOX-loaded NSL along with concurrent NIR treatment could lead to better tumoricidal efficacy than either liposomal DOX medication or sole photothermal ablation. The experimental results indicate that the NSL system developed in this study is a promising candidate for safe and effective combinational anticancer therapy, while the therapeutic efficiency and safety concerns will be evaluated and optimized on more advanced and complex cancer models. The therapeutic strategy described in this study could also be extended for the implementation of other hydrophobic photoactive therapeutic agents, showing clinical interest in future phototherapeutic applications.

4. Experimental Section

Materials: Cationic heptamethine indocyanine dye IR825 was prepared according to the literature report.[11] All chemicals were used as received without further purification. Phospholipids, i.e., DPPC and DSPC, were purchased from Nippon Oil & Fats Co. Ltd. Japan, and 1,2-distearoyl-sn-glycero-3-phosphoethanolamine-N-PEG2000 (DSPE-PEG2000) and liposome mini-extruder (pore size: 100 nm) were provided by Avanti Polar Lipids. Chloroform and methanol were purchased from Merck. All other chemicals not mentioned here were purchased from Sigma-Aldrich. Sephadex PD-10 columns were purchased from GE healthcare.

Preparation of the NSL: The NSL containing DPPC:DSPC:DSPE-PEG_{2000}:IR825 in a weight ratio of 55 mg:20 mg:27 mg:10 mg was prepared using the conventional film-hydration and sonication method. All the lipids were predissolved in the mixture solution of chloroform and methanol (volume ratio 4:1) together with IR825. The mixture was subsequently evaporated under vacuum on a rotary evaporator to form a homogenous lipid film. The lipid film was then hydrated with aqueous solution (19 mL) containing dextrose (1 g) and DOX (95 mg) at pH 7.2 and 60 °C for 30 min. The as-prepared multilaminar liposomes were then sonicated using a probe tip sonicator for 30 min, and subsequently extruded 21 times through the polycarbonate filter of 100 nm (the barrel of the extruder was heated to 60 °C), leading to small unilaminar liposomes with an average diameter of less than 100 nm. Noting that the raw product was centrifuged under 10 000 rpm for 10 min before extrusion in order to remove the titanium scraps and liposome aggregates. Nonentrapped DOX was removed from the liposome solution by passing through a PD-10 Sephadex column just before usage. Size distribution and zeta potential (ζ) were measured by dynamic light scattering using a Malvern Zetasizer Nano ZS. TEM images of the NIR-absorptive stealth liposomes were taken on a JEOL 2010 analytical TEM.

Differential Scanning Calorimetry: The critical temperature for the phase transition of the lipid bilayer was measured using differential scanning calorimetry (DSC) with a Capillary Cell MicroCalorimeter (MicroCal VP-DSC). Empty aluminum hermetic sample pans of the same model were airtightly sealed and used as the reference. The liposome solution was heated from 30 to 70 °C with a heating rate of 1 °C min^{-1}.

Optical Characterization of IR825 and the NSL: UV–vis absorption spectra of photothermal dye IR825 and NSL were recorded on a Shimadzu UV-3600 UV–vis–NIR spectrophotometer in a 1 mm quartz cell. Specifically for the dye IR825 itself, it was first dissolved in methanol (IR825 concentration: 0.01 mg mL^{-1}) and then measured on the spectrophotometer. For nonloaded NSL and DOX-loaded NSL, they were diluted with the aqueous solution of dextrose (dextrose concentration: 5% w/w) in a 1:4 volume ratio. It should be mentioned that the DOX-loaded NSL was purified through the PD-10 column passage using the gravity protocol before the measurement, which was to eliminate the optical interference of nontrapped DOX in the solution.

Determination of the DOX Encapsulation Amount in the NSL: The loading amount of DOX into the NSL was determined by the standard-curve calibration method. Basically, purified DOX-loaded NSL solution (10 µL) containing lipids (60 µg) was added into a detergent solution (990 µL, deionized water containing 2% Triton-100) and subsequently incubated at 55 °C under dark environment for 30 min. The DOX fluorescence reading of the solution was then quantified using a standard curve of DOX in water, which would give the actual DOX concentration in the liposome/detergent mixture. The NSL encapsulation efficiency was then calculated as the ratio of [DOX]/[DOX-loaded NSL].

Characterization for Photothermal Capability of the NSL: Original NSL solution (250 µL) was diluted to 1 mL using dextrose aqueous solution (5% w/w), and the solution was transferred to a quartz cuvette, capped and wrapped with parafilm airtightly. This preparation procedure was used to eliminate the possible increase of liposome concentration caused by the solvent evaporation during the photothermal heating. To maximize effective absorbing area, the cuvette was positioned at a 45° angle. The NIR laser source was placed directly above the cuvette and the power density of the incoming NIR laser was fixed at 0.5 W cm^{-2}. Equal volume of dextrose solution was used as the experimental control. The temperature of each sample was recorded using a noncontact infrared thermometer to ensure the accuracy of the measurements.

Evaluation of the Thermostability and Photothermal-Induced Drug Release: The release profile measurement was achieved using the dialysis method. In brief, DOX-loaded NSL solution (400 µL) was first passed through a PD-10 column and subsequently poured into a cuvette. The cuvette was then illuminated with NIR laser for varied durations using a same protocol as the above photothermal measurements. When the illumination was complete, the solution was again transferred into a dialysis bag (molecular weight cut off 10 kDa, SpetrumLabs). The dialysis system containing photothermal-treated liposomes was suspended in a release medium of dextrose solution (40 mL, weight fraction 5%) at 4 °C, which was gently rotated at 100 rpm in order to ensure that the DOX concentrations in the donor and acceptor compartments were at an equilibrium stage to prevent continuous DOX release during the dialysis. After 20 min, the release medium (1 mL) was collected for the fluorescence detection. For the control group, instead of laser illumination, the cuvette with purified DOX-loaded NSL solution was heated at 37 °C in equal durations, and the sample-processing procedure was the same to other experimental groups.

Investigation on Cellular Uptake of the NSL: The cellular uptake of the NSL was qualitatively investigated by confocal laser microscope and fluorescent anticancer drug DOX was used as the tracer agent. HeLa cells were first incubated with either DOX-loaded NSL (200 µg mL^{-1}) or free DOX (3 µg mL^{-1}) for 4 h. Subsequently, the drug-containing media

were decanted and the cell films were washed twice with phosphate-buffered saline (PBS) to remove the liposomes and free DOX that were not internalized by the cells during the incubation. The washed cells were then fixed with 4% paraformaldehyde for 15 min and washed twice again with PBS. The nuclei of the fixed cells were stained with H33258 (w/v: 2 μg mL^{-1}) at room temperature for 20 min and the cell samples were inspected by confocal laser microscope within 30 min.

Flow Cytometry Analysis of the NSL Internalization and DOX-Induced Apoptosis: The cellular uptake of the NSL and its proapoptotic effects were quantified by flow cytometry. HeLa cells were seeded in a six-well plate with a density of 2×10^5 cells per well. To ensure the adequate cell adhesion to the plate surface, the seeded cells were first incubated at 37 °C for 24 h. Subsequently, for the experimental groups, the culture media were replaced with media containing DOX-loaded NSL, where the liposome concentration was adjusted to 200 μg mL^{-1}. For the control groups, the media were just replaced with fresh ones. Throughout the incubation, the total volumes of the culture media were kept at 2 mL. After another 4 h of incubation, the cells were washed with PBS twice and detached with trypsin solution. The detached cells were then stained by Annexin V FITC following the protocol provided in the Dead Cell Apoptosis Kit (Invitrogen) and had their fluorescence intensity measured on a flow cytometer. All samples were measured within 30 min after the staining, and 1×10^4 events were recorded for each sample.

Cytotoxicity Assessment of the NSL In Vitro: The cytotoxicity assessment of the NSL was conducted on the HeLa cell line using MTT assay. HeLa cells were incubated with either nonloaded NSL or DOX-loaded NSL at different concentrations for 4 h and then washed with fresh medium. For the experimental groups, the cells were subsequently illuminated with NIR laser at 808 nm for 5 or 10 min and the power density of the NIR laser was fixed at 0.5 W cm^{-2}. Cell samples without NIR treatment were used as the negative control. Both sample groups were incubated at 37 °C for another 24 h. The optical density (OD) of the samples at 570 nm was recorded using a plate reader.

Combinational Therapy on Zebrafish Hyperplasia Model: Transgenic zebrafish embryos expressing EGFP-$kras^{v12}$ oncogene were treated with mifepristone to induce the liver hyperplasia as described previously.[41] Induction with mifepristone (1×10^{-6} M, from Sigma-Aldrich) was carried out for 4 d, where liver tumors can be observed in most treated larvae. Liver tumor-bearing larvae were then mounted in 1% low melting agarose, with the liver and heart facing upward for direct injection of respective samples into the liver. Confocal microscopic images of the liver tumors were acquired using an upright Zeiss Axiovert 200M laser scanning microscope (LSM Meta 510, Carl Zeiss). Detection of the tracing agent and EGFP was enabled with two excitation laser lines (30 mW argon and 1 mW HeNe) and emission band-pass filters of 505 nm/530 nm and 560 nm/615 nm that visualize EGFP-$kras^{v12}$ and internalized fluorescence tracer, respectively. All mounted zebrafish were imaged immediately after the injection. The same larvae were imaged again 1 d after the injection. All images were acquired under the same acquisition settings. Quantification of liver tumor volume was achieved with Volumest plugin in Image J.

Supporting Information

Supporting Information is available from the Wiley Online Library or from the author.

Acknowledgements

This work was supported by the National Research Foundation (NRF), Prime Minister's Office, Singapore under its NRF Fellowship (NRF2009NRF-RF001-015) and Campus for Research Excellence and Technological Enterprise (CREATE) Programme–Singapore Peking University Research Centre for a Sustainable Low-Carbon Future, the NTU-A*Star Silicon Technologies Centre of Excellence under the program Grant No. 112351500003, and the NTU-Northwestern Institute for Nanomedicine. Transgenic zebrafish based mifepristone-inducible liver tumor models expressing the EGFP-$kras^{v12}$ oncogene were maintained in the zebrafish facility of Institute of Molecular and Cell Biology Singapore and utilized with their permission. Zebrafish based experiments were carried out in accordance with the Institutional Animal Care and Use Committee (IACUC) approved protocol (IACUC application No. 120787).

Received: June 17, 2015
Revised: July 13, 2015
Published online: August 12, 2015

[1] X. Huang, I. H. El-Sayed, W. Qian, M. A. El-Sayed, *J. Am. Chem. Soc.* **2006**, *128*, 2115.
[2] J. R. Melamed, R. S. Edelstein, E. S. Day, *ACS Nano* **2015**, *9*, 6.
[3] C. Holohan, S. Van Schaeybroeck, D. B. Longley, P. G. Johnston, *Nat. Rev. Cancer* **2013**, *13*, 714.
[4] P. B. Garcia-Allende, J. Glatz, M. Koch, J. J. Tjalma, E. Hartmans, A. G. T. Terwisscha van Scheltinga, P. Symvoulidis, G. M. van Dam, W. B. Nagengast, V. Ntziachristos, *Biomed. Opt. Express* **2014**, *5*, 78.
[5] M. Watanabe, H. Takemura, H. Mizoguchi, H. Hyodo, K. Soga, T. Zako, H. Kishimoto, M. Ito, K. Kaneko, in *The 15th International Conference on Biomedical Engineering*, Vol. 43, (Ed: J. Goh), Springer International Publishing, Cham, Switzerland, **2014**, p. 128.
[6] H. Ke, J. Wang, Z. Dai, Y. Jin, E. Qu, Z. Xing, C. Guo, X. Yue, J. Liu, *Angew. Chem. Int. Ed.* **2011**, *50*, 3017.
[7] L. Cheng, K. Yang, Y. Li, J. Chen, C. Wang, M. Shao, S.-T. Lee, Z. Liu, *Angew. Chem. Int. Ed.* **2011**, *50*, 7385.
[8] K. Yang, S. Zhang, G. Zhang, X. Sun, S.-T. Lee, Z. Liu, *Nano Lett.* **2010**, *10*, 3318.
[9] Q. Tian, F. Jiang, R. Zou, Q. Liu, Z. Chen, M. Zhu, S. Yang, J. Wang, J. Wang, J. Hu, *ACS Nano* **2011**, *5*, 9761.
[10] X. Song, Q. Chen, Z. Liu, *Nano Res.* **2015**, *8*, 340.
[11] L. Cheng, W. He, H. Gong, C. Wang, Q. Chen, Z. Cheng, Z. Liu, *Adv. Funct. Mater.* **2013**, *23*, 5893.
[12] X. Song, H. Gong, T. Liu, L. Cheng, C. Wang, X. Sun, C. Liang, Z. Liu, *Small* **2014**, *10*, 4362.
[13] Q. Chen, C. Wang, L. Cheng, W. He, Z. Cheng, Z. Liu, *Biomaterials* **2014**, *35*, 2915.
[14] W. T. Al-Jamal, K. Kostarelos, *Acc. Chem. Res.* **2011**, *44*, 1094.
[15] T. M. Allen, P. R. Cullis, *Adv. Drug Delivery Rev.* **2013**, *65*, 36.
[16] Š. Koudelka, J. Turánek, *J. Controlled Release* **2012**, *163*, 322.
[17] D. L. Emerson, *Pharm. Sci. Technol. Today* **2000**, *3*, 205.
[18] Y. Barenholz, *J. Controlled Release* **2012**, *160*, 117.
[19] R. W. Horne, A. D. Bangham, V. P. Whittaker, *Nature* **1963**, *200*, 1340.
[20] B. Čeh, M. Winterhalter, P. M. Frederik, J. J. Vallner, D. D. Lasic, *Adv. Drug Delivery Rev.* **1997**, *24*, 165.
[21] M. L. Immordino, F. Dosio, L. Cattel, *Int. J. Nanomed.* **2006**, *1*, 297.
[22] M. Silvander, M. Johnsson, K. Edwards, *Chem. Phys. Lipids* **1998**, *97*, 15.
[23] P. Crosasso, M. Ceruti, P. Brusa, S. Arpicco, F. Dosio, L. Cattel, *J. Controlled Release* **2000**, *63*, 19.
[24] T. Ta, E. Bartolak-Suki, E.-J. Park, K. Karrobi, N. J. McDannold, T. M. Porter, *J. Controlled Release* **2014**, *194*, 71.
[25] L. Li, T. L. M. Ten Hagen, D. Schipper, T. M. Wijnberg, G. C. van Rhoon, A. M. M. Eggermont, L. H. Lindner, G. A. Koning, *J. Controlled Release* **2010**, *143*, 274.
[26] G. A. Koning, A. M. M. Eggermont, L. H. Lindner, T. L. M. Ten Hagen, *Pharm. Res.* **2010**, *27*, 1750.

[27] B. M. Dicheva, T. L. M. T. Hagen, L. Li, D. Schipper, A. L. B. Seynhaeve, G. C. V. Rhoon, A. M. M. Eggermont, L. H. Lindner, G. A. Koning, *Nano Lett.* **2012**, *13*, 2324.
[28] V. P. Torchilin, *Nat. Rev. Drug Discovery* **2005**, *4*, 145.
[29] X. Ma, C. Teh, Q. Zhang, P. Borah, C. Choong, V. Korzh, Y. Zhao, *Antioxid. Redox Signaling* **2013**, *21*, 707.
[30] L. Vuković, F. A. Khatib, S. P. Drake, A. Madriaga, K. S. Brandenburg, P. Král, H. Onyuksel, *J. Am. Chem. Soc.* **2011**, *133*, 13481.
[31] B. M. Dicheva, T. L. M. Ten Hagen, D. Schipper, A. L. B. Seynhaeve, G. C. Van Rhoon, A. M. M. Eggermont, G. A. Koning, *J. Controlled Release* **2014**, *195*, 37.
[32] L. Li, T. L. M. Ten Hagen, M. Hossann, R. Süss, G. C. van Rhoon, A. M. M. Eggermont, D. Haemmerich, G. A. Koning, *J. Controlled Release* **2013**, *168*, 142.
[33] J. P. May, S.-D. Li, *Recent Pat. Biomed. Eng.* **2012**, *5*, 148.
[34] X.-B. Xiong, Y. Huang, W.-L. Lu, X. Zhang, H. Zhang, T. Nagai, Q. Zhang, *J. Controlled Release* **2005**, *107*, 262.
[35] A. Jhaveri, P. Deshpande, V. Torchilin, *J. Controlled Release* **2014**, *190*, 352.
[36] J. P. May, M. J. Ernsting, E. Undzys, S.-D. Li, *Mol. Pharm.* **2013**, *10*, 4499.
[37] T. Ta, T. M. Porter, *J. Controlled Release* **2013**, *169*, 112.
[38] Y. Zhao, Z. Luo, M. Li, Q. Qu, X. Ma, S.-H. Yu, Y. Zhao, *Angew. Chem. Int. Ed.* **2015**, *54*, 919.
[39] Z. Luo, X. Ding, Y. Hu, S. Wu, Y. Xiang, Y. Zeng, B. Zhang, H. Yan, H. Zhang, L. Zhu, J. Liu, J. Li, K. Cai, Y. Zhao, *ACS Nano* **2013**, *7*, 10271.
[40] M. R. Hamblin, T. N. Demidova, *Proc. SPIE* **2006**, *6140*, 1.
[41] A. T. Nguyen, A. Emelyanov, C. H. V. Koh, J. M. Spitsbergen, S. Parinov, Z. Gong, *Dis. Models & Mech.* **2012**, *5*, 63.